A Deeper Look into Thiophene Coordination Prior to Oxidative Addition of the C−S Bond to Platinum(0): A Computational Study Using DFT and MO Methods

Tülay A. Ateşin and William D. Jones*

Department of Chemistry, University of Rochester, Rochester, New York 14627

Received July 6, 2007

The reaction of thiophene with a zerovalent platinum bisalkylphosphine fragment yields a highly stable thiaplatinacycle derived from cleavage of the C−S bond. Calculations on the [Pt(dmpe)] model system using Density Functional Theory are consistent with experimental results obtained with [Pt(dippe)] in that the reaction is exothermic overall and furthermore predict that the initial η^2-coordination of thiophene through the C═C double bond is energetically more favorable than coordination through the sulfur atom (ΔG = 9.3 kcal/mol). There are three well-defined transition states along the pathway to the oxidative addition product from both of these coordination modes. Two of these lead to a higher energy η^2-C,S-coordinated intermediate, while the third one leads to cleavage of the C−S bond from the η^2-C,S complex. As the reaction was carried out in a polar solvent (THF), the effect of solvation was taken into account by using the polarizable continuum model. The thermodynamic preference for the initial coordination of thiophene through the C═C bond is found to be greater in THF (ΔG = 11.4 kcal/mol). More importantly, the total free energy of the transition state from the C═C coordinated complex is now lower than that of the S-coordinated complex in solution. Therefore, the initial η^2-coordination of thiophene through the C═C double bond results in the kinetically preferred pathway. Molecular orbital analyses were carried out to rationalize the results.

Introduction

Hydrodesulfurization (HDS) is the process through which sulfur-containing compounds are removed from natural gas and refined petroleum products.[1] Because currently available technologies are no longer sufficient for the "deep refining" needed to meet more severe limitations on the amount of the sulfur,[2] a renewed interest in HDS catalysis research incorporating different disciplines is indispensable. A significant amount of research has focused on homogeneous models of HDS catalysts due to the difficulty in understanding the mechanism of the heterogeneous process.

In these models, the reactions of metal complexes with thiophene and substituted thiophene were studied, and important mechanistic pathways were proposed. These include the π-coordination of thiophene either through one double bond[3] or through the whole of its π system.[4] Alternatively, initial coordination through sulfur to form a S-bound complex,[5] leading to insertion of the metal into the C−S bond, has been proposed.[6]

Density Functional Theory (DFT) offers a powerful tool for the detailed study of organometallic systems in order to understand their reactivity and structure. More importantly, DFT is able to predict both reaction and activation energies reliably and accurately, thus enabling the study of the kinetics and thermodynamics of individual organometallic reactions involved in a catalytic cycle. Prior theoretical treatments of C−S bond cleavage in thiophenes have been reported for homogeneous metal complexes such as $[Mn(CO)_4]$,[7] [Cp*Rh(PMe_3)],[8] [Ni(dmpe)],[9] and [Ir(triphos)],[10] for small clusters such as Ni_3S_2,[11]

* To whom correspondence should be addressed. E-mail: jones@chem.rochester.edu.

(1) Schuman, S. C.; Shalit, H. *Catal. Rev.* **1970**, *4*, 245.

(2) Sanchez-Delgado, R. A. *Organometallic Modeling of the Hydrodesulfurization and Hydronitrogenation Reactions*; Kluwer Academic Publishers: Dordrecht, 2002; p 1.

(3) Kwart, H.; Schuit, G. C. A.; Gates, B. C. *J. Catal.* **1980**, *61*, 128.

(4) (a) Schoofs, G. R.; Preston, R. E.; Benziger, J. B. *Langmuir* **1985**, *1*, 313. (b) Lockemeyer, J. R.; Rauchfuss, T. B.; Rheingold, A. L.; Wilson, S. R. *J. Am. Chem. Soc.* **1989**, *111*, 8828. (c) Lesch, D. A.; Richardson, J. W.; Jacobson, R. A.; Angelici, R. J. *J. Am. Chem. Soc.* **1984**, *106*, 2901. (d) Hachgenei, J. W.; Angelici, R. J. *Organometallics* **1989**, *8*, 14. (e) Spies, G. H.; Angelici, R. J. *Organometallics* **1987**, *6*, 1897. (f) Hachgenei, J. W.; Angelici, R. J. *J. Organomet. Chem.* **1988**, *355*, 359. (g) Chen, J.; Angelici, R. J. *Organometallics* **1989**, *8*, 2277. (h) Ogilvy, A. E.; Skaugset, A. E.; Rauchfuss, T. B. *Organometallics* **1989**, *8*, 2739.

(5) (a) Kolboe, S. *Can. J. Chem.* **1969**, *47*, 352. (b) Choi, M.-G.; Angelici, R. J. *J. Am. Chem. Soc.* **1989**, *111*, 8753. (c) Draganjac, M.; Ruffing, C. J.; Rauchfuss, T. B. *Organometallics* **1985**, *4*, 1909. (d) Kuehn, C. G.; Taube, H. *J. Am. Chem. Soc.* **1976**, *98*, 689. (e) Wasserman, J. J.; Kubas, G. J.; Ryan, R. R. *J. Am. Chem. Soc.* **1986**, *108*, 2294. (f) Goodrich, J. D.; Nickias, P. N.; Selegue, J. P. *Inorg. Chem.* **1987**, *26*, 3424. (g) Kuhn, N.; Schumann, H. *J. Organomet. Chem.* **1984**, *276*, 55. (h) Catheline, D.; Astruc, D. *J. Organomet. Chem.* **1984**, *272*, 417. (i) Guerchais, V.; Astruc, D. *J. Organomet. Chem.* **1986**, *316*, 335.

(6) (a) Jones, W. D.; Dong, L. *J. Am. Chem. Soc.* **1991**, *113*, 559. (b) Dong, L.; Duckett, S. B.; Ohman, K. F.; Jones, W. D. *J. Am. Chem. Soc.* **1992**, *114*, 151.

(7) Li, H.; Yu, K.; Watson, E. J.; Virkaitis, K. L.; D'Acchioli, J. S.; Carpenter, G. B.; Sweigart, D. A.; Czech, P. T.; Overly, K. R.; Coughlin, F. *Organometallics* **2002**, *21*, 1262.

(8) (a) Sargent, A. L.; Titus, E. P. *Organometallics* **1995**, *17*, 65. (b) Maresca, O.; Maseras, F.; Lledüs, A. *New J. Chem.* **2004**, *28*, 625. (c) Blonski, C.; Myers, A. W.; Palmer, M.; Harris, S.; Jones, W. D. *Organometallics* **1997**, *16*, 3819. (d) Palmer, M. S.; Rowe, S.; Harris, S. *Organometallics* **1998**, *17*, 3798.

(9) Palmer, M.; Harris, S. *Organometallics* **2000**, *19*, 2114.

(10) Palmer, M.; Carter, K.; Harris, S. *Organometallics* **1997**, *16*, 2448.

(11) Neurock, M. *Appl. Catal., A* **1997**, *160*, 169.

10.1021/om700679j CCC: $40.75
Publication on Web 12/20/2007

and on heterogeneous surfaces of particles of MoCoS,[12] in which a variety of mechanisms were proposed.

Recently, platinum has emerged as a feasible catalyst for the industrial HDS process.[13] A full homogeneous HDS sequence mediated by platinum has been demonstrated by Garcia from the reversible reaction of the platinum(0) complex $Pt(PEt_3)_3$ with thiophene.[14] In this reaction, platinum metal oxidatively inserts into one of the C−S bonds to give a six-membered thiaplatinacycle, which then extrudes S to give the parent hydrocarbon.

Previously, we have published the effect of the d^8 transition metals on the activation of thiophenic C−S bonds and the electronic structure of the thiophene metallacycles formed.[15] Both experimental and DFT show that the thiaplatinacycle, which is formed from oxidative addition of the C−S bond to the platinum fragment, is more stable than its nickel and palladium analogues. In this paper, the DFT calculations on the reaction of thiophene with the [Pt(dmpe)] fragment as a model for the experimental reactions of Pt[(dippe)] will be presented to probe the mechanism by which thiophene reacts with the metal center. The structural aspects of thiophene binding by σ-complexation of S and η^2 π-complexation of C═C were considered as the initial coordination modes of thiophene prior to insertion of the metal into the C−S bond. To the best of our knowledge, this is the first theoretical study on the bond activation of thiophene that demonstrates the critical importance of taking into account the effect of solvation.

Results and Discussion

When thiophene was added to a THF solution of $[Pt(dippe)H]_2$, clean formation of the C−S oxidative addition product (**1**) was observed at elevated temperatures (>60 °C) (eq 1):[15]

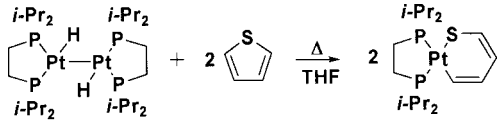

1

(1)

The lack of observation of any reaction intermediates makes DFT calculations necessary to investigate the mechanism of this bond cleavage process. To simplify the calculations, the *i*-Pr groups in the [Pt(dippe)] fragment were substituted by methyl groups. This simplification is assumed to have no steric outcome on the calculations, as the single crystal X-ray structures showed no interaction between the methyl groups of the dippe ligand and the thiophene ring.[15]

The known experimental structure for the oxidative addition product, whose ORTEP drawing is shown in Figure 1, was used as the starting point for all calculations. To choose the best

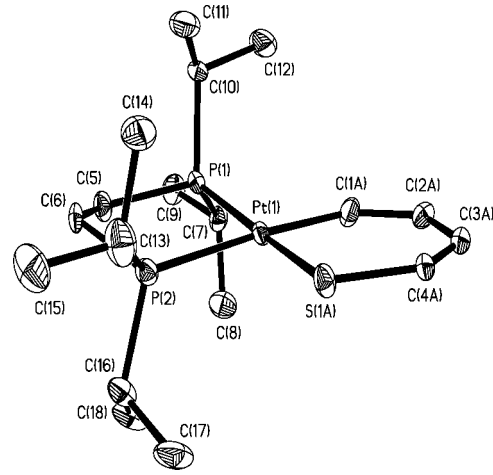

Figure 1. ORTEP drawing of **1**. Ellipsoids are shown at the 30% probability level. All hydrogen atoms are omitted for clarity. Disorder isomer ratio (fraction of major): 0.642(12).

method for the modeling, several exchange and correlation functions were used to calculate the ΔG of the reaction shown in eq 2:

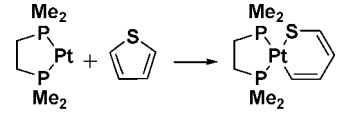

S1

(2)

Selected optimized structural parameters and the energy of formation of the oxidative addition product with the different exchange and correlation functionals are summarized in Table 1, along with the structural parameters obtained from X-ray. The crystals of **1** contained a disordered molecule in the asymmetric unit as a result of the interchange of the position of the sulfur atom in the metal-inserted thiophenic ring. Although the structure of **1** was successfully refined, this disorder rendered the metrical parameters of only modest value for comparison purposes only.[15] All of the functionals are consistent with the exothermicity of the reaction and give similar optimized structural features consistent with the crystal structure, such as square-planar geometry around the metal center and coplanar thienyl ligand. Clear bond-length alternation (short–long–short) within the thiophenic ring is also predicted by all of the functionals. The C1−C2 and C3−C4 bond lengths are indicative of a C═C double bond, and those of C2−C3 are indicative of a C−C single bond. Although the thiophenic carbon−carbon bond lengths of **1** obtained from the solid-state structure have a longer C1−C2 bond implying electron delocalization, the optimized structures show a localized double bond. This result is consistent with the bond lengths reported for the substituted thiaplatinacycles in the literature.[16] As no significant difference was obtained by using the different functionals, we used B3LYP, which is currently the most widely used method.[17]

The optimized structure of the oxidative addition product was used as the starting point for the C−S bond cleavage transition-

(12) Lauritsen, J. V.; Nyberg, M.; Vang, R. T.; Bollinger, M. V.; Clausen, B. S.; Topsøe, H.; Jacobsen, K. W.; Lægsgaard, E.; Nørskov, J. K.; Besenbacher, F. *Nanotechnology* **2003**, *14*, 385.

(13) (a) van den Berg, J. P.; Lucien, J. P.; Germaine, G.; Thielemans, G. L. B. *Fuel Process. Technol.* **1993**, *35*, 119. (b) Cooper, B. H.; Stanislaus, A.; Hannerup, P. N. *Hydrocarbon Process.* **1993**, (June), 83. (c) Maxwell, I. E.; Naber, J. E.; de Jong, K. P *Appl. Catal., A* **1994**, *113*, 153. (d) Mignard, S.; Marchal, N.; Kasztelan, S. *Bull. Soc. Chim. Belg.* **1995**, *104*, 259.

(14) (a) García, J. J.; Mann, B. E.; Adams, H.; Bailey, N. A.; Maitlis, P. M. *J. Am. Chem. Soc.* **1995**, *117*, 2179. (b) Garcia, J. J.; Maitlis, P. M. *J. Am. Chem. Soc.* **1993**, *115*, 12200.

(15) Atesin, T. A.; Oster, S. S.; Skugrud, K.; Jones, W. D. *Inorg. Chim. Acta* **2006**, *359*, 2798.

(16) (a) Garcia, J. J.; Arevalo, A.; Capella, S.; Chehata, A.; Hernandez, M.; Montiel, V.; Picazo, G.; Del Rio, F.; Toscano, R. A.; Adams, H.; Maitlis, P. M. *Polyhedron* **1997**, *16*, 3185. (b) Garcia, J. J.; Arevalo, A.; Montiel, V.; Del Rio, F.; Quiroz, B.; Adams, H.; Maitlis, P. M. *Organometallics* **1997**, *16*, 3216.

(17) Cundari, T. R. *Computational Organometallic Chemistry*; Marcel Dekker Inc.: New York, NY, 2001; pp 72.

Table 1. Selected Optimized Structures of S1, X-ray Structure of 1, and Energy of Formation (Δ*G*, kcal/mol) of Oxidative Addition Product of the Reaction [Pt(dmpe)] + Thiophene[a]

	Pt−P1	Pt−P2	Pt−C1	C1−C2	C2−C3	C3−C4	C4−S	Pt−S	P1−Pt−P2	S−Pt−C1	Δ*G*[b]
BLYP	2.315	2.401	2.037	1.376	1.444	1.371	1.749	2.359	85.499	94.006	−27.9
B3LYP	2.296	2.376	2.025	1.363	1.440	1.358	1.736	2.338	85.625	94.030	−29.3
BP86	2.287	2.363	2.021	1.376	1.439	1.371	1.739	2.331	85.735	94.401	−32.6
B3P86	2.271	2.343	2.010	1.362	1.434	1.356	1.726	2.312	85.811	94.362	−33.7
BPW91	2.287	2.363	2.021	1.374	1.438	1.370	1.737	2.330	85.676	94.272	−30.0
B3PW91	2.275	2.349	2.013	1.363	1.435	1.357	1.728	2.316	85.770	94.235	−31.0
BVWN	2.328	2.421	2.044	1.372	1.445	1.368	1.749	2.371	85.318	93.632	−20.8
X-ray	2.277 (2)	2.290 (3)	1.930 (3)	1.405 (3)	1.425 (3)	1.345 (3)	1.712 (3)	2.322 (3)	87.72 (5)	95.10 (3)	

[a] Gibbs free energies in gas phase, 1 atm, 298 K (0.04 M). [b] Distances are in Å, and angles are in deg. Atom numbering is as shown in Figure 1.

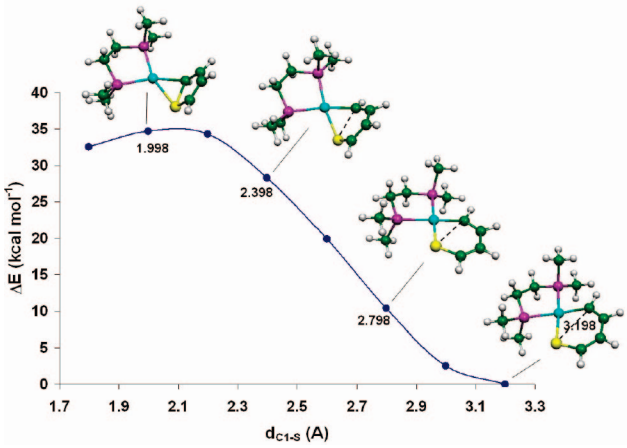

Figure 2. Locating the C−S cleavage transition state, **TS12**.

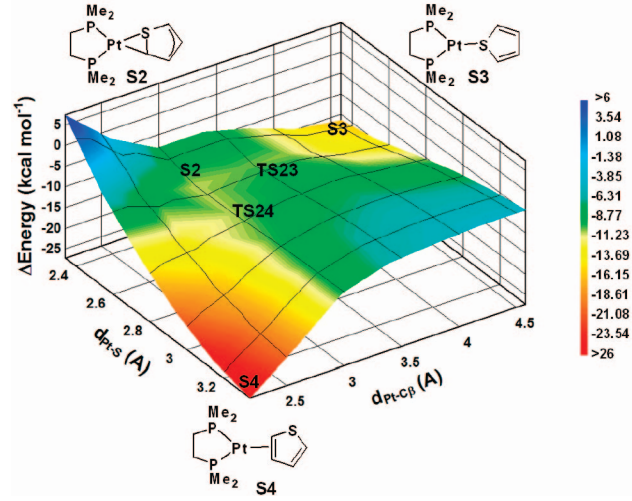

Figure 3. Potential energy surface scan along the Pt-S and Pt-C_β bonds.

state calculations. A relaxed potential energy surface scan was done with the initial value of the C−S bond at 3.198 Å, which is the distance between the carbon atom bound to the platinum and the sulfur atom in the optimized oxidative addition product structure, and decreasing it with a step size of 0.2 Å a total of seven times. A geometry optimization was performed for each resulting structure. The energy of the optimized structures with these restrained C−S bond lengths initially increased and reached a maximum between d_{C-S} = 2.198 and 1.998 Å (Figure 2). The transition state for the C−S bond cleavage (**TS12**) was located by taking the optimized structure around the energy maximum and optimizing it as a transition state. From the optimized transition-state structure, the forward and the reverse intrinsic reaction coordinate (IRC) calculations were performed to find out which coordination mode of the thiophene to the metal center leads to the bond cleavage product. In the forward direction, the reaction path leads to the oxidative addition product, whereas in the reverse direction it leads to a stable η^2-C,S adduct (**S2**), which is not one of the expected coordination modes of the thiophene reported in the literature.[18]

The coordination mode of thiophene to the platinum(0) fragment is crucial to understanding the mechanism of the HDS process. This unprecedented high energy η^2-C,S coordination of thiophene to the [Pt(dmpe)] fragment leaves open the question of whether thiophene initially coordinates to the metal center through its C=C double bond or its S atom prior to C−S bond cleavage.[19] To look for further interactions between the thiophene ring and the [Pt(dmpe)] fragment, the ground-state structures of S- and η^2-C,C-coordinated thiophenes (**S3** and **S4**, respectively) were optimized and a potential energy surface (PES) scan was carried out by varying the distance between the platinum metal and the sulfur atom (d_{Pt-S}) and the distance between the platinum metal and the β-carbon atom (C2) ($d_{Pt-C\beta}$) of the thiophene molecule (Figure 3). Two energy minima were found corresponding to the S-coordinated and the η^2-C,C-coordinated thiophene complexes, both of which are substantially lower in energy than the η^2-C,S-coordinated thiophene.

No transition state directly connecting the S- and the η^2-C,C-coordinated thiophenes was located. Instead, two different transition states connecting the S- and η^2-C,C-coordinated thiophenes to the η^2-C,S-coordinated intermediate were found. The one from the S-coordinated thiophene (**TS23**) was located by using the QST2 method and confirmed with an IRC calculation. For the η^2-C,C to η^2-C,S transition (**TS24**) QST2 was unable to locate the correct transition state.[20] Therefore it was found using an approach similar to that employed in finding the C−S bond cleavage transition state. The optimized structure of the η^2-C,C intermediate was used as the starting point for this calculation. A relaxed potential energy surface scan was performed by setting the initial value of the Pt−S bond to 3.391 Å and decreasing it with a step size of 0.13 Å a total of seven times, performing an optimization for each resulting geometry. The energy of the optimized structures reached a maximum around d_{C-S} = 2.611 Å (Figure 4). The transition state was found by taking the optimized structure around the energy maximum and optimizing it as a transition state. The forward and the reverse IRC calculations confirmed that it joins η^2-C,C- and η^2-C,S-coordinated thiophene complexes.

(18) Angelici, R. J. *Acc. Chem. Res.* **1988**, *21*, 387.

(19) Due to the relatively high energy of the η^2-C,S-coordinated thiophene compared to the S- or η^2-C,C coordinated complexes, it is not likely that thiophene initially binds via its S−C σ bond, but instead through the more accessible sulfur lone pair or the C=C double bond.

(20) The IRC calculations done on this transition state show that it leads to rotation around the C=C double bond in the η^2-C,C coordinated thiophene.

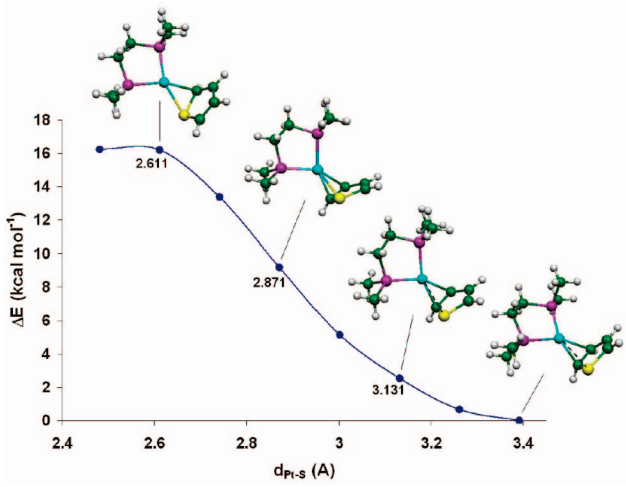

Figure 4. Locating the transition state from η^2-C,C- to η^2-C,S-coordinated thiophene.

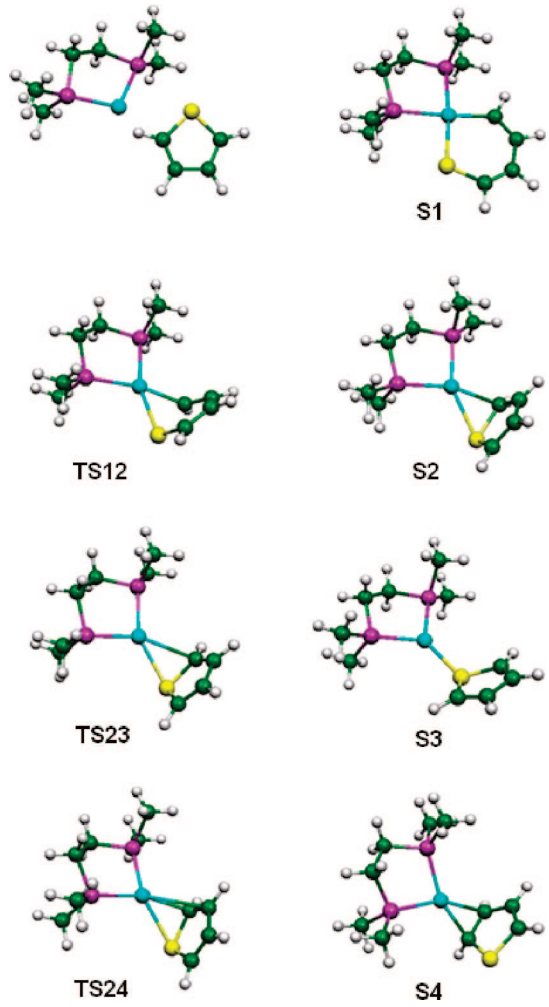

Figure 5. Optimized structures of stationary points on the [Pt(dmpe)] + thiophene potential energy surface.

The optimization of all of the above ground-state and the transition-state structures (**S1-S4** and **TS12-TS24**) were done in the gas phase. These optimized structures are shown in Figure 5, and their structural parameters are given in Table 2. As the experimental studies were carried out in a polar solvent (THF), these calculated structures were also optimized using the polarizable continuum model (PCM). The PCM optimized structural parameters are given in Table 3. Although the structural differences are minimal, the energies of the species change by up to 15 kcal/mol. In the discussions of the structures that follow, we will use the gas-phase geometries.

In the oxidative addition product **S1**, the metal has inserted between the C1 and the S atom to form a square planar complex. The breaking of the bond is complete, as reflected by the S−C1 distance, which is about 3.20 Å. The six-membered ring adopts a planar geometry and has clear bond-length alternation (short–long–short) within the thiophenic ring. The C1−C2 and C3−C4 bond lengths are indicative of a C=C double bond and those of C2−C3 are indicative of a C−C single bond. The Pt−C1 and Pt−S bond lengths are 2.025 and 2.338 Å, respectively.

In η^2-C,S-coordinated complex **S2**, although thiophene binds to the metal center in a π-fashion through its C−S bond between the C1 and S atoms, the lengthening of the C−S bond is insignificant (1.819 Å). Here, the Pt−C1 and Pt−S distances are 2.208 and 2.544 Å, respectively, only about 0.2 Å longer than those found in the oxidative addition product. Furthermore, C1 has lost much of its sp^2 hybridization to become more like an sp^3 carbon.[21] The bonded thiophene molecule is at an angle of 120° to the P−Pt−P plane. The π system is involved in the bonding, as the S−C1, C1−C2, C2−C3, and C3−C4 bond lengths are different in comparison with those in free thiophene. The C1−C2 bond length (1.429 Å) is closer to a C−C single bond, whereas C2−C3 and C3−C4 bond lengths (1.395 and 1.392 Å) are in between C−C single bond and C=C double bond, indicating electron delocalization between C2, C3, and C4.

The η^1 character of **S3** is evident from the short Pt−S distance of about 2.34 Å and the two long Pt−C1 and Pt−C4 distances of about 3.59 Å. The η^1 coordination does not affect the π system of the thiophene, and the S−C1 and S−C4 bond lengths before and after binding are nearly the same. The bound thiophene molecule is at an angle of 140.5° to the P−Pt−P plane.

In complex **S4**, thiophene binds to the metal center through its π bond between the C1 and C2 atoms in an η^2 fashion. The Pt−C1 and Pt−C2 distances are short, 2.120 and 2.158 Å, respectively, and the Pt−S distance is long (around 3.39 Å). Both C1 and C2 have lost much of their sp^2 hybridization to become more like sp^3 carbons. The C1−C2 bond length (1.458 Å) is consistent with a C−C single bond. The S−C1 bond is slightly lengthened (1.816 Å). The bound thiophene molecule is now at an angle of 114° to the P−Pt−P plane. The formal oxidation number of the metal is equal to 2 in the oxidative addition product, whereas it is equal to 0 in the η^1 and the η^2 coordination complexes.

Examination of the transition state for the C−S bond cleavage shows that the S−C1 bond length in **TS12** (2.089 Å) is significantly lengthened from its value in the initial complex **S2** (1.819 Å). The Pt−C1 and Pt−S bond lengths (2.113 Å and 2.398 Å, respectively) are close to their value in the final insertion complex **S1**. The formation of the Pt−C1 and Pt−S bonds are thus more advanced than the breaking of the S−C1 bond in this transition state. The C1−C2, C2−C3, and C3−C4 bond lengths are all between C−C single bond and C=C double bond, which indicates extensive electron delocalization between these atoms.

Starting with the stable olefin complex, **S4**, the Pt−S distance is dramatically shortened to reach transition state **TS24**. The thiophene molecule is tilted because of its rotation around the

(21) The sum of angles H−C1−S, H−C1−C2, and S−C1−C2 is 345.8°, a value between an sp^2 carbon (360°) and an sp^3 carbon (327°).

Table 2. Gas-Phase Optimized Structures and Relative Gibbs Free Energies (Δ*G*, kcal/mol) of Stationary Points on the [Pt(dmpe)] + Thiophene Potential Energy Surface[a]

	Pt−S	Pt−C1	Pt−C2	S−C1	C1−C2	C2−C3	C3−C4	C4−S	Δ*G*
S1	2.338	2.025	3.079	3.198	1.363	1.440	1.358	1.736	−29.28
TS12	2.398	2.113	3.155	2.089	1.402	1.410	1.379	1.747	3.17
S2	2.544	2.208	3.159	1.819	1.429	1.395	1.392	1.733	−0.06
TS23	2.532	2.653	3.529	1.763	1.388	1.418	1.376	1.744	1.88
S3	2.340	3.590	4.585	1.754	1.363	1.438	1.363	1.754	−5.16
TS24	2.635	2.181	2.973	1.806	1.428	1.405	1.384	1.735	1.57
S4	3.391	2.120	2.158	1.816	1.458	1.467	1.350	1.767	−14.40

[a] Distances are in Å. Atom numbering is as shown in Figure 1.

Table 3. Optimized Structures with PCM in THF and Relative Total Free Energies in Solution (Δ*G*, kcal/mol) of Stationary Points on the [Pt(dmpe)] + Thiophene Potential Energy Surface[a]

	Pt−S	Pt−C1	Pt−C2	S−C1	C1−C2	C2−C3	C3−C4	C4−S	Δ*G*
S1	2.349	2.031	3.088	3.206	1.365	1.444	1.358	1.744	−42.38
TS12	2.402	2.115	3.164	2.041	1.412	1.406	1.384	1.750	−2.25
S2	2.506	2.186	3.168	1.832	1.434	1.394	1.397	1.741	−3.73
TS23	2.512	2.685	3.581	1.764	1.390	1.419	1.378	1.747	−2.78
S3	2.327	3.626	4.642	1.757	1.364	1.439	1.364	1.757	−20.34
TS24	2.684	2.148	2.880	1.810	1.434	1.409	1.382	1.742	0.03
S4	3.399	2.109	2.148	1.825	1.464	1.469	1.350	1.775	−8.95

[a] Distances are in Å. Atom numbering is as shown in Figure 1.

Pt−C1 axis in order to bring the sulfur atom closer to the Pt atom. The Pt−C2 bond length is substantially longer.

Transition state **TS23** joining the S-bound and η^2-C,S-bound thiophene complexes results from the rotation of thiophene in its molecular plane in **S3** in order to reduce the Pt−C1 distance to form the Pt−C1 bond. The thiophene molecule is quite perpendicular at an angle of about 100° to the P−Pt−P plane. C1 shows evidence of possessing partial sp^3 character. The S−C1 bond length in **TS23** (1.763 Å) is not so different from its value in the initial complex **S3** (1.754 Å), and the Pt−C1 and Pt−S bond lengths (2.653 and 2.532 Å, respectively) are closer to their value in the η^2-C,S-coordinated complex **S2** (2.208 and 2.544 Å).

In all of the transition-state structures described above, the C2−C3 bond length is considerably shorter and the C3−C4 bond length is considerably longer than those in free thiophene; therefore a delocalization of electron density between C2, C3, and C4 atoms is shown in the figures representing these transition states. The relative energies of the optimized structures were calculated with respect to the free fragments. All three transition states were found to be higher in energy than the total energy of free fragments (Figure 6), indicating dissociation of thiophene from [Pt(dmpe)] fragment during these interconversions. However, when solvation in THF is taken into account using PCM,[22] the energetics change significantly (Figure 7). As a result of the large polarity differences of the platinum−thiophene complexes, they are stabilized by THF to different extents. The polar oxidative addition product, **S1**, and the transition state leading to this product, **TS12**, were stabilized the most. The C═C double bond coordinated thiophene, **S4**, and the transition state from this intermediate, **TS24**, were stabilized to a lesser extent, whereas the S-coordinated thiophene, **S3**, and the transition state from this intermediate, **TS23**, were the least stabilized platinum−thiophene complexes as they are the least polar. The transition state between the S-coordinated thiophene to η^2-C,S-coordinated thiophene, **TS23**, is found to be still above the total energy of the free fragments in PCM calculations, demonstrating the dissociative nature of this interconversion.

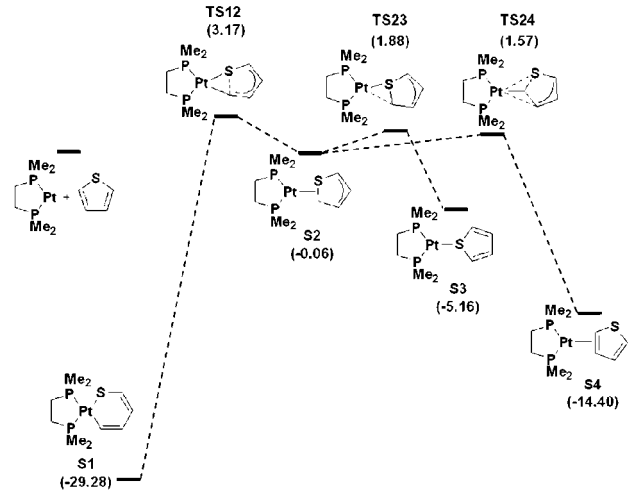

Figure 6. Energetics of C−S bond activation of thiophene by [Pt(dmpe)] (free energies in kcal/mol at 298 K) relative to the total energies of fragments ([Pt(dmpe)] and thiophene) in the gas phase.

Both **TS12** and **TS24** are found to be below the dissociation limit. Therefore we propose that the reaction of thiophene with [Pt(dippe)] fragment proceeds via initial coordination of thiophene through the C═C double bond. Migration of the metal toward the S atom of the thiophene leads to the formation of the high energy η^2-C,S-coordinated thiophene and the oxidative addition takes place through this intermediate. In this scheme, the S-bound species, **S3**, represents a "dead-end" intermediate.

The optimized structural parameters calculated in THF with PCM are tabulated in Table 3. There is not a significant change in bond lengths between the gas-phase optimized structures and those in Table 3.

MO Analysis. The fragment molecular orbital approach, which considers the symmetry and energy requirements for the possible donation and back-donation interactions, was used to analyze the electronic structures of **S1**, **S3**, and **S4**.[23] The

(22) This model treats the solvent as a sphere of the appropriate size that is rolled over the surface of the molecule, with the dipole of the solvent interacting optimally to stabilize the molecule. Miertus, S.; Scrocco, E.; Tomasi, J *Chem. Phys.* **1981**, *55*, 117.

(23) (a) Gorelsky S. I. *AOMix: Program for Molecular Orbital Analysis*; York University: Toronto, Canada, 1997; http://www.sg-chem.net/. (b) Gorelsky, S. I.; A, B. P.; Lever, J. *Organomet. Chem.* **2001**, *635*, 187–196.

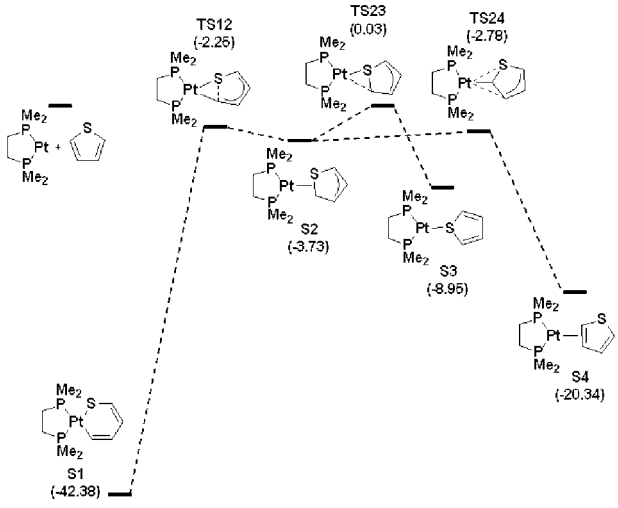

Figure 7. Energetics of C−S bond activation of thiophene by [Pt(dmpe)] (free energies in kcal/mol at 298.15 K) relative to the total energies of fragments ([Pt(dmpe)] and thiophene) with PCM solvation correction in THF.

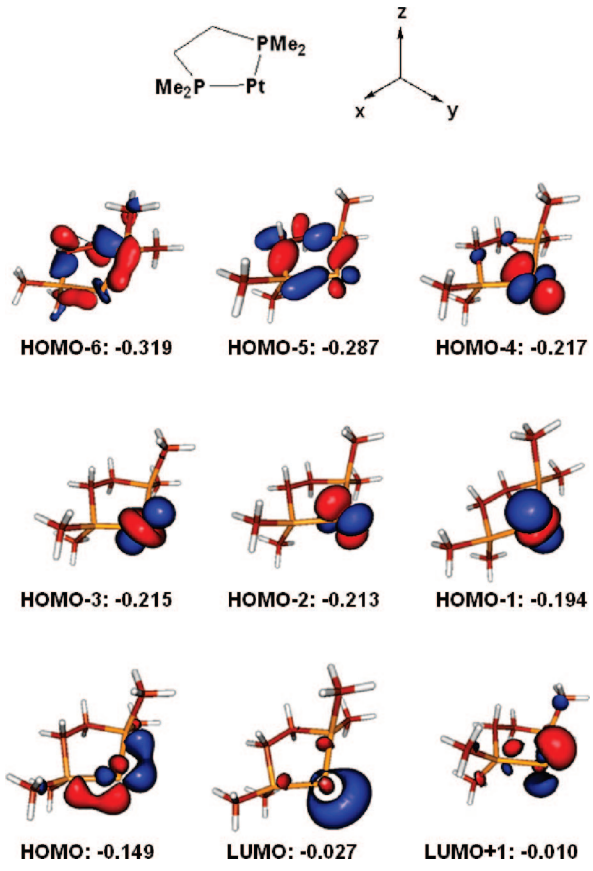

Figure 8. Selected MOs for [Pt^0(dmpe)] fragment, their corresponding energies (eV), and the chosen coordinate system. The *x* and *y* axes are in-plane, the *z* axis is perpendicular to the *xy* plane.

oxidative addition product of the C−S bond cleavage was used as the starting point for these analyses. The bonding interactions in **S1** were further used to rationalize the relative stabilities of the other platinum−thiophene species. The molecular orbitals were calculated for the [Pt(dmpe)] fragment (Figure 8) and the open thiophene fragment (Figure 9), as this is the geometry of the thiophene ring in the C−S bond cleavage product.

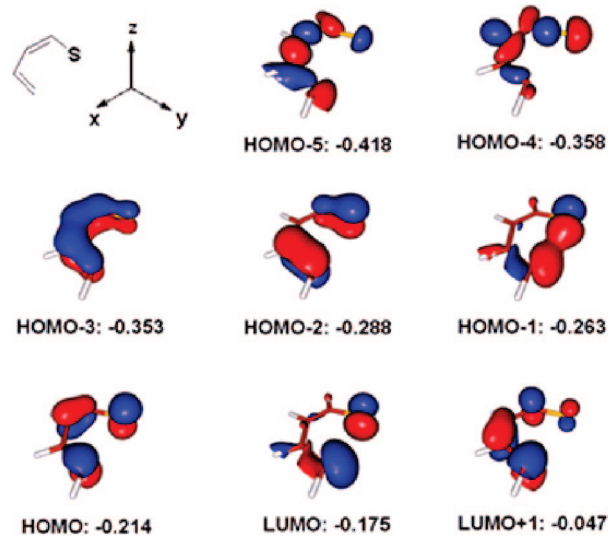

Figure 9. Selected MOs of the open neutral thiophene fragment, their corresponding energies (eV), and the chosen coordinate system. The *x* and *y* axes are in-plane, the *z* axis is perpendicular to the *xy* plane.

The electron density of the frontier molecular orbitals of the [Pt(dmpe)] fragment is localized mainly on the platinum atom. The HOMO (highest occupied molecular orbital) is predominantly the d_{xy} orbital with some p_x mixing (see Figure 8 for the definition of the coordinate system). The HOMO-1 is the d_{z^2} orbital with some *s* mixing. The HOMO-2 is the d_{yz} orbital, the HOMO-3 is mainly the d_{xz} orbital with some $d_{x^2-y^2}$ mixing and the HOMO-4 is the $d_{x^2-y^2}$ orbital with some d_{xz} mixing. Both the HOMO-5 and HOMO-6 are mainly the Pt−P σ bonding orbitals. The LUMO (lowest unoccupied molecular orbital) is the s-p_y hybrid orbital directed toward the incoming thiophene ligand, and it is in the plane of the ligand ring system, whereas the LUMO+1, which has a π orbital symmetry perpendicular to the ligand ring system, is mainly the p_z orbital with some d_{yz} mixing.

The HOMO in the neutral opened thiophene fragment is a π orbital perpendicular to the plane of the ring system. The electron density of this orbital is mainly localized on the sulfur atom with significant π electron density on the terminal carbon atom. The HOMO-1 and the LUMO in the ring-opened thiophene are both σ orbitals containing electron density on both the sulfur and the terminal carbon atom. The HOMO-1 is bonding with respect to the C−S interaction while the LUMO is antibonding. The HOMO-3, HOMO-2, HOMO, and the LUMO+1 are all π orbitals perpendicular to the ring system.

The important bonding interactions between the metal and the thiophene fragment in **S1** are summarized in Figure 10. The interaction of the HOMO on the Pt^0 and the LUMO of the thiophene fragment gives rise to one σ-bonding MO (HOMO-3), and the interaction of the HOMO on the fragment and the LUMO on the metal give rise to a second σ-bonding MO (HOMO-4). One other MO (HOMO-17) also shows some σ-bonding character. The HOMO and HOMO-1 in **S1** are π-antibonding between the Pt and the thiophene fragment, consistent with the notion that this is not a delocalized π-system.

The molecular orbitals of thiophene were calculated to examine the bonding interactions between the thiophene and the [Pt(dmpe)] fragment before the bond cleavage (Figure 11). The frontier molecular orbitals of the thiophene are π in character. The LUMO+1 is in the plane of the thiophene ring and σ^* antibonding between the sulfur and the adjacent carbon

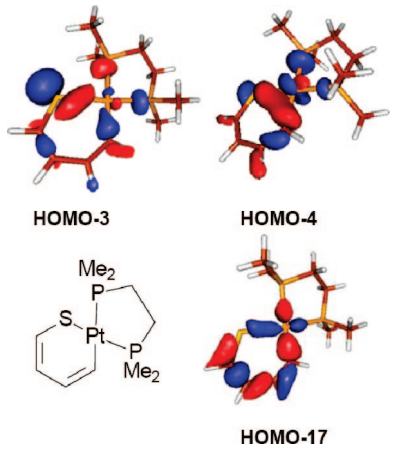

Figure 10. Important bonding interactions between the metal fragment and the thiophene ligand in **S1**.

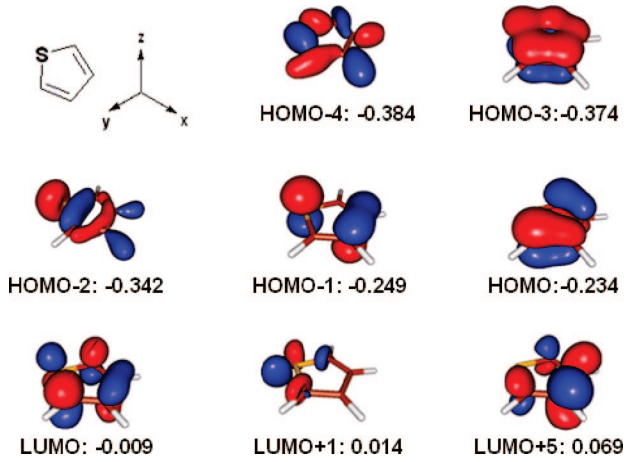

Figure 11. Selected MOs for thiophene, their corresponding energies (eV), and the chosen coordinate system. The *x* and *y* axes are in-plane; the *z* axis is perpendicular to the *xy* plane.

atoms and consists of the *s* and p_x orbitals of the α-carbons and p_y orbital of the sulfur atom. The HOMO-2 and HOMO-4 are the C−S σ bonding interactions. The HOMO-2 consists of the p_x orbitals of the α-carbons, p_x, p_y orbitals of the β-carbons and *s*, p_x orbitals of the sulfur atom, and the HOMO-4 consists of the same *p* orbitals of the α- and β-carbons and the p_y orbital of the sulfur atom.

The molecular orbitals involved in thiophene binding are summarized below. As the thiophene geometry in **S3** is not distorted as in the other complexes formed, the bonding interactions between the metal fragment and the thiophene ligand in S-bound complex **S3** are discussed first.

The molecular orbitals of **S3** with considerable electron density between the platinum and the sulfur atom are summarized in Figure 12. Remarkably, most of the MOs show no interaction between the thiophene and the metal. However, HOMO-6 shows some σ-bonding character between Pt and sulfur, as does HOMO-17. The PtP_2 LUMO, while of the proper symmetry for σ-bonding, is ineffective as an acceptor for the sulfur lone pair electrons. (See Supporting Information for compositions of MOs in terms of dominant fragment orbital contributions). Coordination of thiophene through sulfur atom to the [Pt(dmpe)] fragment forms a very weak complex (~9 kcal/mol), which is evident from the lack of effective back-bonding, thus no strong Pt−S bonding interaction occurs.

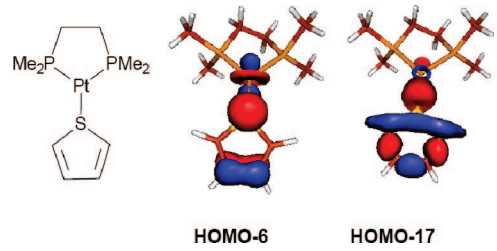

Figure 12. Important bonding interactions between the metal fragment and the thiophene ligand in **S3**.

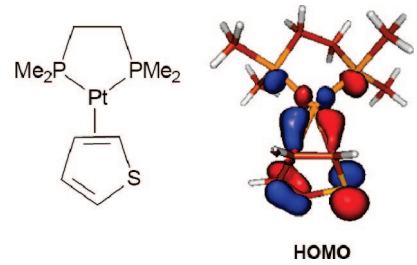

Figure 13. Important bonding interactions between the metal fragment and the thiophene ligand in **S4**.

The MO showing the bonding interactions between the platinum and the double bond carbons in **S4** is shown in Figure 13. The HOMO is formed from π-backbonding from the metal d_{xy} orbital (HOMO) to a thiophene C−C π^* orbital (LUMO). Donation from the C−C π-bonding orbital to the metal is ineffective for bonding due to the filled nature of all five *d*-orbitals. Once again, the PtP_2 LUMO is also ineffective as an acceptor for the C−C π-bonding electrons. (See Supporting Information for compositions of MOs in terms of dominant fragment orbital contributions). The back-donation of electron density from the metal to the thiophene ligand is the main stabilizing interaction in **S4**, which is lacking in **S3**, thereby accounting for the greater stability of **S4**.

Conclusions

The reaction of thiophene with the [Pt(dippe)] fragment yields a highly stable C−S bond cleavage product. DFT calculations on the model system using a [Pt(dmpe)] fragment predict exothermic C−S bond activation both in the gas phase and in THF with PCM correction for polarity, and the energetically more favorable η^2-coordination of thiophene through its C=C double bond. Due to the large energy difference between η^2-C,C, η^2-C,S and S coordination modes, we propose that thiophene exclusively coordinates to the platinum fragment through its C=C double bond. Two well-defined transition states were located on the potential energy surface between the η^2-C,C- and S-coordinated thiophene intermediates and the C−S bond activation product. The first leads to a higher energy η^2-C,S-coordinated intermediate, while the second leads to cleavage of the C−S bond from the latter complex. The Gibbs free energies calculated for all three transition states are found to be higher than the total energy of the free fragments, indicating that these species may interconvert by way of dissociation/reassociation. When the reaction pathway was modeled with a PCM correction, it was found out that there is a considerable solvation effect on the energetics of C−S bond cleavage. This is attributed to the large polarity differences between the intermediates and the transition states found on the [Pt(dmpe)] + thiophene potential energy surface. In solution, the thermodynamic preference for the initial coordination of thiophene

through the C═C bond is found to be greater in THF (ΔG = 9.7 kcal/mol). More importantly, the total free energies of the transition state from the C═C coordinated complex and the transition state for the C−S bond cleavage are now lower than the total free energies of fragments in solution by 2.2 and 2.8 kcal/mol, respectively. The total free energy of the transition state joining the S-coordinated complex and the η^2-C,S-coordinated intermediate is found to be essentially the same as that of the fragments, indicating that interconversion of these species may proceed by way of a dissociative pathway. Therefore, the initial η^2-coordination of thiophene through the C═C double bond results in the only kinetically accessible pathway. It is clear from the DFT calculations on the model system that the reaction of thiophene with [Pt(dippe)] fragment proceeds via initial η^2-coordination of thiophene through C═C double bond. Migration of the metal toward the S atom of the thiophene leads to the formation of the high energy η^2-C,S-coordinated thiophene intermediate and the oxidative addition takes place through this intermediate. Molecular orbital (MO) analyses support the relative energetics of these compounds.

Computational Methods

When available, known experimental structures for the complexes were used as the starting point for the calculations. To simplify these calculations, the *i*-Pr groups were substituted by methyl groups. This simplification is assumed to have no steric outcome on the calculations, as the X-ray single crystal structures showed no interaction between the methyl groups and the thiophene ring. The gas-phase structures were fully optimized in redundant internal coordinates,[24] with DFT and a wave function incorporating Becke's three-parameter hybrid functional (B3),[25] along with the Lee–Yang–Parr correlation functional (LYP).[26] All calculations were performed using the Gaussian03[27] package. The Pt, P, and S atoms were represented with the effective core pseudopotentials of the Stuttgart group, and the associated basis sets were improved with a set of f-polarization functions for the transition metal (α = 0.993, Pt)[28] and a set of d-polarization functions for the main group elements (α = 0.387, P; α = 0.503, S).[29] The remaining atoms (C and H) were represented with 6-31G(d,p)[30] basis sets. The geometry optimizations were performed without any symmetry constraints. The transition state connecting the S- and η^2-C,S-coordinated thiophenes was located with the QST2 method. The optimized geometries for the reactant (S-coordinated thiophene) and the product (η^2-C,S-coordinated thiophene) were used for this kind of transition state optimization. QST2 generates a guess for the transition structure that is midway between the reactants and products in terms of redundant internal coordinates, and it then goes on to optimize that starting structure to a first-order saddle point automatically. The local minima and the transition states were checked by frequency calculations. For each transition-state structure, the intrinsic reaction coordinate (IRC) routes were calculated in both directions toward the corresponding minima. For some of the transition states, the IRC calculations failed to reach the energy minima on the potential energy surface; therefore, in those cases geometry optimizations were carried out as a continuation of the IRC path. Because of the polarity of the structures, the solvent effects on their relative stabilities were evaluated by calculating the free energies of solvation in terms of the polarizable continuum model (PCM).[5] The self-consistent reaction field (SCRF) calculations using the PCM-UA0 solvation model[31] were carried out for the PCM optimized structures. The dielectric constant in the PCM calculations was set to ϵ = 7.58 to simulate THF as the solvent medium used in the experimental study.[1] The energies discussed throughout the text are electronic energies without any ZPE corrections. Gibbs free energies have been calculated at 298.15 K and 1 atm. The fragment molecular analyses were carried out by the AOMix-CDA package of programmes.[23] The Molden package was used to display the molecular orbitals and the electron densities.[32]

Acknowledgment. We would like to acknowledge the NSF for financial support (CHE-0414325 and CHE-0717040). We thank Sébastien Lachaize for helpful discussions on how to set the PES job and Abdurrahman Atesin for MO analysis.

Supporting Information Available: Optimized geometries of the ground-state (**S1**−**S4**) and transition-state structures (**TS12**, **TS23**, **TS24**) as well as the fragments with PCM and in gas phase, portions of Gaussian input files for the geometry optimizations with PCM and the compositions of MOs in terms of dominant fragment orbital contributions for **S1**, **S3**, and **S4**. This material is available free of charge via the Internet at http://pubs.acs.org.

OM700679J

(24) Peng, C.; Ayala, P. Y.; Schlegel, H. B.; Frisch, M. J. *J. Comput. Chem.* **1996**, *17*, 49.
(25) Becke, A. D. *J. Chem. Phys.* **1993**, *98*, 5648.
(26) Lee, C.; Yang, W.; Parr, R. G. *Phys. Rev. B* **1988**, *37*, 785.
(27) Frisch, M. J.; Trucks, G. W.; Schlegel, H. B.; Scuseria, G. E.; Robb, M. A.; Cheeseman, J. R.; Montgomery, Jr., J. A.; Vreven, T.; Kudin, K. N.; Burant, J. C.; Millam, J. M.; Iyengar, S. S.; Tomasi, J.; Barone, V.; Mennucci, B.; Cossi, M.; Scalmani, G.; Rega, N.; Petersson, G. A.; Nakatsuji, H.; Hada, M.; Ehara, M.; Toyota, K.; Fukuda, R.; Hasegawa, J.; Ishida, M.; Nakajima, T.; Honda, Y.; Kitao, O.; Nakai, H.; Klene, M.; Li, X.; Knox, J. E.; Hratchian, H. P.; Cross, J. B.; Bakken, V.; Adamo, C.; Jaramillo, J.; Gomperts, R.; Stratmann, R. E.; Yazyev, O.; Austin, A. J.; Cammi, R.; Pomelli, C.; Ochterski, J. W.; Ayala, P. Y.; Morokuma, K.; Voth, G. A.; Salvador, P.; Dannenberg, J. J.; Zakrzewski, V. G.; Dapprich, S.; Daniels, A. D.; Strain, M. C.; Farkas, O.; Malick, D. K.; Rabuck, A. D.; Raghavachari, K.; Foresman, J. B.; Ortiz, J. V.; Cui, Q.; Baboul, A. G.; Clifford, S.; Cioslowski, J.; Stefanov, B. B.; Liu, G.; Liashenko, A.; Piskorz, P.; Komaromi, I.; Martin, R. L.; Fox, D. J.; Keith, T.; Al-Laham, M. A.; Peng, C. Y.; Nanayakkara, A.; Challacombe, M.; Gill, P. M. W.; Johnson, B.; Chen, W.; Wong, M. W.; Gonzalez, C.; and Pople, J. A. *Gaussian03*; Gaussian, Inc.: Wallingford, CT, 2004.
(28) Ehlers, A. W.; Bohme, M.; Dapprich, S.; Gobbi, A.; Hollwarth, A.; Jonas, V.; Kohler, K. F.; Stegmann, R.; Veldkamp, A.; Frenking, G. *Chem. Phys. Lett.* **1993**, *208*, 111.
(29) Hollwarth, A.; Bohme, M.; Dapprich, S.; Ehlers, A. W.; Gobbi, A.; Jonas, V.; Kohler, K. F.; Stegmann, R.; Veldkamp, A.; Frenking, G. *Chem. Phys. Lett.* **1993**, *208*, 237.
(30) Hehre, W. J.; Ditchfield, R.; Pople, J. A. *J. Chem. Phys.* **1972**, *56*, 2257.
(31) Barone, V.; Cossi, M.; Tomasi, J. *J. Chem. Phys.* **1997**, *107*, 3210.
(32) Schaftenaar, G.; Noordik, J. H. *J. Comput.-Aided Mol. Des.* **2000**, *14*, 123.